Magnesium Technology 2014
Edited by: Martyn Alderman, Michele V. Manuel, Norbert Hort, and Neale R. Neelameggham
TMS (The Minerals, Metals & Materials Society), 2014

EFFECT OF SURFACE CONDITION ON THE LOCALIZED CORROSION BEHAVIOR OF MAGNESIUM ALLOY AZ31B

Z.P. Cano, J.R. Kish, J.R. McDermid
GM Centre for Automotive Materials & Corrosion, McMaster University, Hamilton, Ontario, Canada L8S 4L7

Keywords: Magnesium, AZ31, Corrosion, Scanning Vibrating Electrode

Abstract

The localized corrosion behavior of AZ31B magnesium alloy sheet was studied in 0.01 M aqueous NaCl solution using the scanning vibrating electrode technique (SVET). Ongoing investigations by the authors have shown significant variation in corrosion mode and relative corrosion resistance depending on the alloy's surface condition. Comparisons were made between the observed behavior of the as-received, acid-cleaned and mechanically-polished surfaces. The SVET work was conducted to elucidate variations in the local electrochemical behavior for each surface condition. SVET maps were coupled with images of the corroding surfaces in order to show the progression of corrosion as a function of time. Schematic corrosion process models are proposed in order to explain the observed differences between the three surface conditions.

Introduction

Magnesium (Mg) alloys have received interest in the automotive industry due to their relatively low weight and favorable strength-to-weight ratio. However, they also have a high reactivity and are, therefore, very susceptible to corrosion when compared to steels and aluminum alloys. This has been a major factor in preventing their widespread adoption into exposed automotive components [1].

The localized corrosion mechanism of magnesium and its alloys continues to be a subject of debate in the scientific literature. Localized corrosion of Mg is often identified as pitting [1,2], but fundamentally different corrosion modes have also been reported. A number of studies over the past 25 years have shown a filiform or thread-like type of corrosion behavior in uncoated Mg [3, 4, 5] and Mg-aluminum (Al) alloys [6, 7].

Williams et al. [5, 7] have used SVET measurements to study filiform-like corrosion on mechanically-polished pure Mg and Mg alloy AZ31. They proposed that this behavior is driven by cathodic activation of the already-corroded areas of the surface, which caused the anodic dissolution to spread laterally across the surface instead of pitting deep into the metal. The cathodic activation in pure Mg was thought to be due to an enrichment of iron (Fe) in the reacted corrosion film, whereas the cathodic activation of AZ31 was thought to be from an enrichment of manganese (Mn)-Al phases.

In this work the localized corrosion behavior of AZ31B Mg alloy sheet taken from an automobile shock tower sub-assembly demo structure was studied. The demo structure was fabricated under the Mg Front End Research and Development (MFERD) project [8, 9]. Using a commercially available scanning electrochemical workstation, SVET measurements were completed to determine how the local electrochemical behavior of the alloy is influenced by its surface condition.

Experimental Procedures

The AZ31B sheet was sectioned into 1 cm × 1 cm square samples and each was cold-mounted in epoxy in order to leave only the plan view surface exposed. Fast-curing epoxy was applied around the edges of the exposed surface to prevent crevice corrosion from occurring at the metal/epoxy interface. All samples were immersed in 0.01 M aqueous NaCl solutions at a neutral pH for 24 h. Three different surface conditions of the alloy were tested and are listed in Table I.

Table I. Tested surface conditions of AZ31B sheet

Test	Surface Condition
1	As-received, ultrasonically cleaned in ethanol
2	Acid-cleaned by immersion of the as-received surface in 10% H_2SO_4 for 20 seconds, rinsed in DI water and ultrasonically cleaned in ethanol
3	Polished to 1200 grit SiC paper with ethanol lubricant

During immersion, local current density values were calculated from the SVET measurements taken as vectors normal to the exposed plan view surface. The SVET involves vibrating a platinum (Pt) electrode tip and measuring the voltage difference between the two extremes of the tip's position. Then, knowing the conductivity of the solution and the amplitude of the tip's vibration, current density can be calculated in the direction of vibration using a modified form of Ohm's law [10]. Alternatively, a calibration relating the measured voltage difference and current density in a given solution can be performed by taking vibrating electrode measurements of a series of known applied current densities [11]. A detailed explanation of the SVET is available elsewhere [10].

SVET measurements were performed using a Princeton Applied Research Model 370 Scanning Electrochemical Workstation. A photograph of the electrode setup is shown in Figure 1. Voltages were measured between the scanning Pt tip and a graphite auxiliary electrode. The diameter of the Pt tip was specified by the manufacturer to be in the range of 5 to 50 μm. SVET scans were completed on a 6 mm × 6 mm area of the sample every 1800 s (30 min.) throughout the duration of each test. The probe outputs were measured using a series of sweeping line scans across the scan area with a speed of 200 μm/s and one data point collected every 150 μm. The probe was vibrated in the vertical direction with an amplitude of 30 μm and a frequency of 80 Hz. The gain of the electrometer was set to 10^4, and the full scale sensitivity of the amplifier was set between 160 μV and 800 μV, depending on the intensity of the voltage signal for each test.

For each full scale sensitivity setting, a calibration test similar to the one outlined by Williams et al. [11] was completed. The vibrating probe was first placed inside a tube with a known inner area. Using a polished gold (Au) working electrode, a series of set

currents were passed through the tube and the vibrating probe output measured for each current. Plots of the probe output verses the set current density were constructed and showed a close linear relationship (the minimum R^2 value was 0.998). An equation relating the two variables was fit to the data in each case and used to convert the local probe outputs from each corrosion test into local current densities.

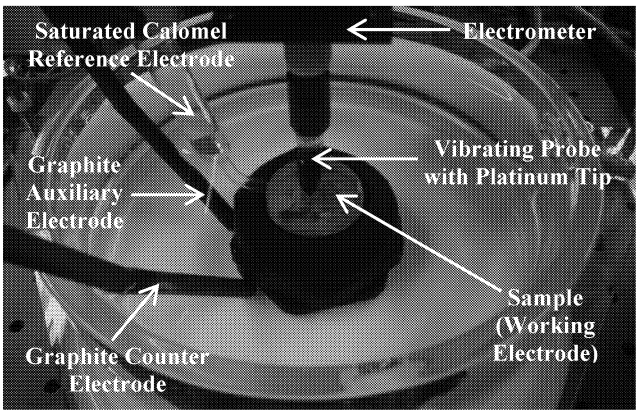

Figure 1. Electrode setup used for SVET measurements.

In order to relate the electrochemical activity with the visual appearance of the localized corrosion, the exposed surfaces were also monitored with a video camera positioned above the cell.

Results

Each surface condition of AZ31B displayed some form of localized corrosion. In two cases there was a delay between the time of immersion and the initiation of localized corrosion; these times are shown in Table II to the nearest half hour.

Table II. Time after immersion until localized corrosion initiation

Test		Time until localized corrosion initiation
1	As-received	Immediate
2	Acid-cleaned	3 h
3	Polished	12.5 h

A series of SVET maps alongside images of the 6 mm × 6 mm scan area for each of the 24-h corrosion tests are presented in Figures 2 through 4. It was not feasible to present every SVET map and image; therefore, those shown were selected to provide a summary of the electrochemical processes and appearance of the sample surfaces evolved as a function of time.

The corrosion reaction of Mg is comprised of the following anodic and cathodic half reactions [2]:

$$Mg \rightarrow Mg^{2+} + 2e^- \quad (1)$$
$$2H_2O + 2e^- \rightarrow H_2 + 2OH^- \quad (2)$$

Reaction (1) causes a positive ionic flow of current (highlighted on the SVET maps in red) while reaction (2) causes a negative ionic flow of current (highlighted on the maps in blue).

As-received AZ31B surface

Numerous hydrogen bubbles were formed on the as-received surface immediately after immersion in 0.01 M NaCl. Dark corroded threads also rapidly formed in the upper right portion of the scan area (Figure 2a). The SVET scans revealed intense

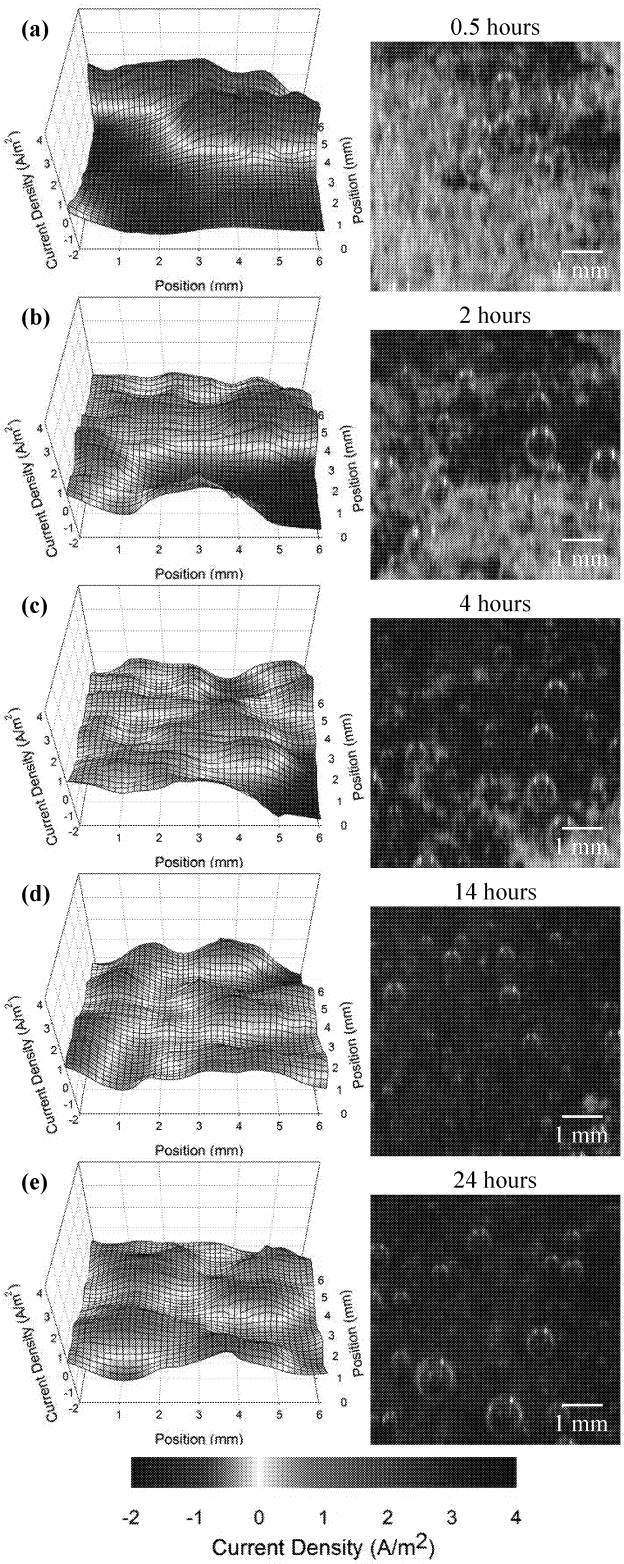

Figure 2. SVET maps and scan area images of the as-received AZ31B surface at various times after immersion in 0.01 M NaCl.

anodic and cathodic coupling across the surface. In the early stages of the test, anodic currents were detected on the corroded areas of the sample and cathodic currents were detected on un-corroded areas (Figure 2a-c). The un-corroded areas produced a relatively constant cathodic current density with an average magnitude of -0.7 A/m^2. Thus, as the surface became increasingly covered by corrosion products, charge neutrality on the surface was maintained by decreasing peak anodic current density magnitudes within the corroded regions. The peak anodic current density was 2.2 A/m^2 after 0.5 h of immersion and slowly decreased to a relatively constant value of 1.0 A/m^2 after the surface was completely covered by corrosion products (after 18 h). The rate at which corrosion products spread across the surface decreased as a function of time, presumably because of diminishing anodic currents.

It is interesting to note that predominantly anodic currents were produced above the dark corroded regions of the as-received AZ31B surface. By contrast, Williams et al. [5, 7, 8] observed predominantly cathodic currents within the corroded regions while anodic currents were only observed at the propagating corrosion front. Anodic currents indicate that Mg is dissolving as Mg^{2+} ions in the corroded areas. This would suggest that corrosion was occurring in a downward direction instead of primarily laterally, the latter of which has been reported for polished surfaces [5, 7, 8].

Using X-ray photoelectron spectroscopy, it was found that the as-received AZ31B surface used in this work contained heavy metal impurities in the native oxide film, including Fe and Cu [12]. As-received AZ31 sheet surfaces are often found to be contaminated with elements such as Cu, Fe and Ni, the latter two arising from the sheet rolling process [13, 14]. Heavy metal particles are well known to act as local cathodes with respect to Mg. It is proposed here that such heavy metal contamination was responsible for the intense microgalvanic activity detected by the SVET measurements on the as-received surface.

Acid-cleaned AZ31B Surface

The acid-cleaned surface did not display any cathodic currents of the magnitude observed for the as-received surface in 0.01 M NaCl. It was, therefore, likely that the acid-cleaning procedure of immersion in 10% H_2SO_4 for 20 seconds succeeded in removing the Fe and Cu particles from the as-received surface.

After immersion in the 0.01M NaCl solution, small bubbles quickly developed across the surface of the sample. Williams et al. [7] observed small SVET-detected cathodic currents above the initially-formed bubbles on polished AZ31 in ~0.9 M NaCl. It was proposed that noble Al-Mn-(Fe) intermetallic particles were present at the surface of these sites and acted as catalysts for reaction (2). However, the SVET maps after initial immersion in this work (not shown) did not display any local anodic or cathodic areas, possibly due to limits of the instrument's sensitivity.

After 3 h, intense hydrogen evolution was observed near the centre of the scan area (Figure 3a). This was accompanied by a local peak in anodic current density of 1.3 A/m^2 from the same area. Filiform-like corrosion then proceeded from several points on the sample in a manner similar to what has been reported in the literature [3-7, 11]. (Figure 3b-e). Hydrogen evolution and a local

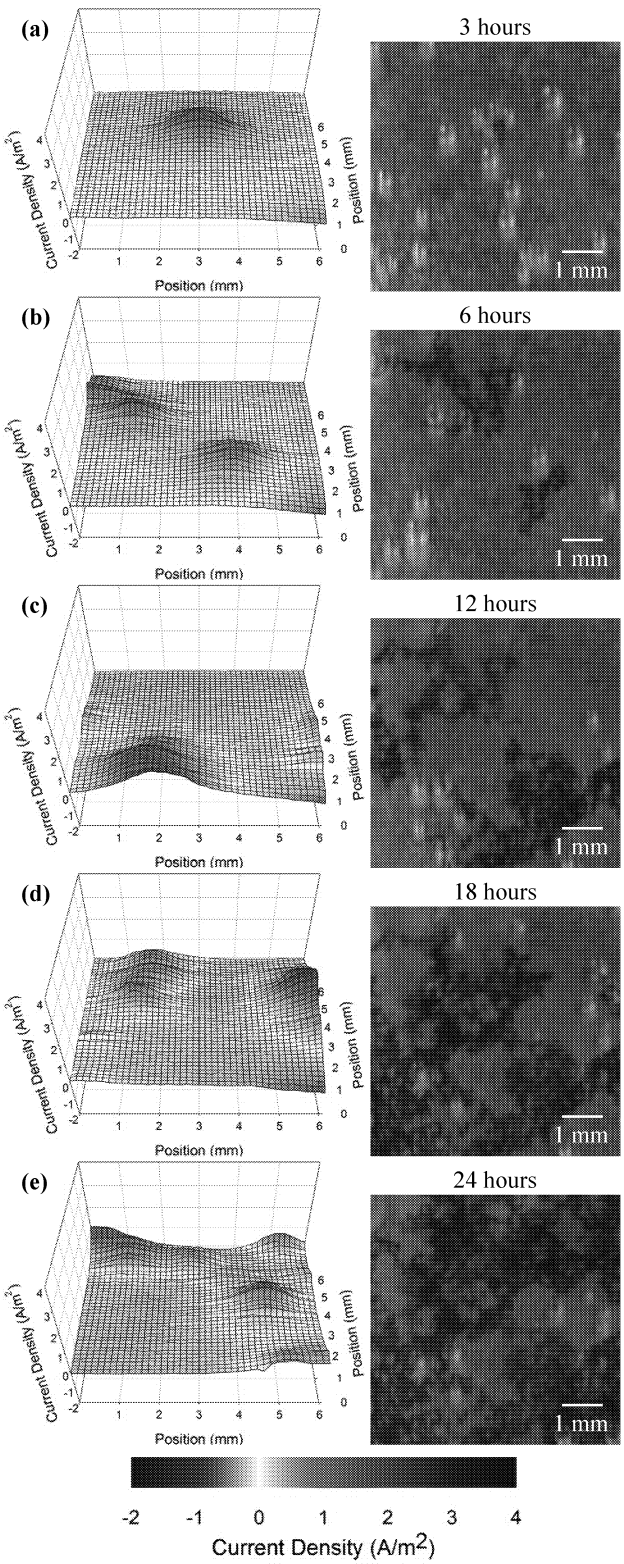

Figure 3. SVET maps and scan area images of the acid-cleaned AZ31B surface at various times after immersion in 0.01 M NaCl.

anodic current density peak were both always observed to occur at the head of a moving filament. This is consistent with the visual observations and SVET measurements of a corroding polished

AZ31 alloy reported by Williams et al. [7], although their study detected much higher anodic current density magnitudes (~100 A/m^2). However, Williams et al. [7] used a much more concentrated salt solution (~0.9 M NaCl) than in this study, which likely contributed to the large current density differences.

Relatively small cathodic currents were detected over the dark corrosion tracks left behind after the filiform-like propagation (Figure 3c-e). In order to maintain the overall charge neutrality on the surface, the intensity of local anodic peaks occurring at the heads of active filaments steadily increased from an average of 0.9 A/m^2 for the first 5 h of localized corrosion to 1.4 A/m^2 during the last 5 h of the test. This was again consistent with the previous report on an AZ31 alloy in ~0.9 M NaCl [7], where the authors showed that the rise in the surface-integrated cathodic current closely matched the rise of surface-integrated anodic current over time.

Test 3 (Polished – 0.01 M NaCl)

As was the case with the acid-cleaned surface, small bubbles quickly developed on the polished surface after immersion. Again, no localized anodic or cathodic currents were detected in the SVET maps (not shown) before the initiation of localized corrosion.

Localized corrosion was initiated just outside the top-left area of the SVET scanned area after 12.5 h. A corrosion filament propagated from this location until it entered the scan area about 1 h later (Figure 4a). The vibrating probe detected a local anodic current density of about 0.8 A/m^2 at the head of the filament. Throughout the rest of the 24-h exposure, multiple filaments were initiated and propagated in the same manner as described for the acid-cleaned sample, matching both its electrochemical behavior and visual appearance (Figure 4b-e).

The only differences between the behavior of the acid-cleaned and polished surfaces was that localized corrosion initiated in the acid-cleaned sample in less than a quarter of the time and propagated at a slightly lower rate. Both of these differences may be attributed to differences in the surface roughness achieved after each preparation procedure. Song et al. [13] reported the surface roughness (Ra) of an AZ31 sample polished to 1200 grit SiC paper to be 0.07 µm, while that for an AZ31 sample immersed in 10% H_2SO_4 for 20 seconds was considerably greater at 2.50 µm. In the same study, the rate of hydrogen evolution in ~0.9 M NaCl was lower on the acid-cleaned sample than the polished sample, which is consistent with the observations here. In another study Walter and Kann [15] reported that the pitting susceptibility of an AZ91 alloy in 0.09 M NaCl increased with increasing surface roughness, which was also consistent with the present results. This finding was attributed to the fact that a smoother surface can form a more continuous protective film than a rough surface [15].

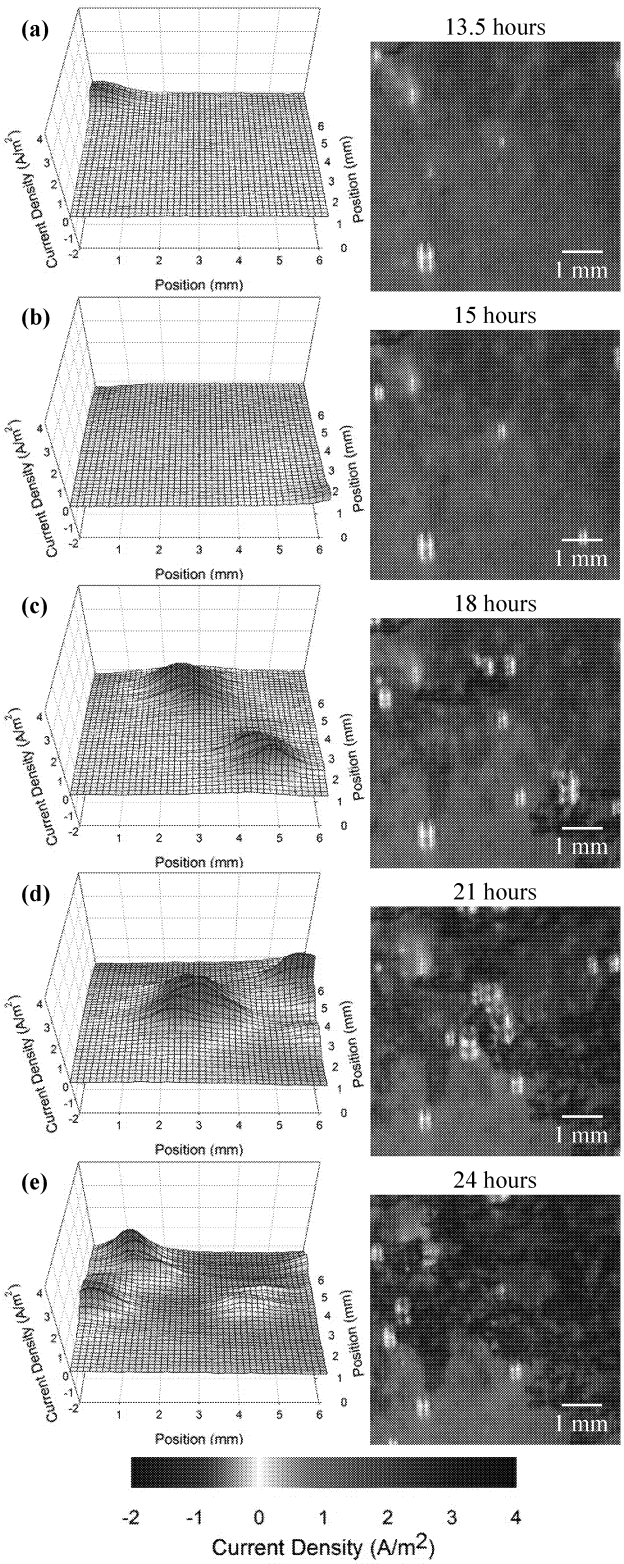

Figure 4. SVET maps and scan area images of the polished AZ31B surface at various times after immersion in 0.01 M NaCl (note that localized corrosion initiated outside of the scan area).

Discussion

In this study the electrochemical behavior of a corroding as-received AZ31B surface was distinctly changed after it was acid-cleaned or mechanically polished. Schematic electrochemical surface profiles are presented in Figure 5 in order to demonstrate the major differences. The polished or acid-cleaned surfaces displayed identical behavior to that reported by Williams et al. [5, 7, 11], where a strong anode at the corrosion front was coupled with a moderately cathodic reacted corrosion film which was left behind in the wake of the moving anode (Figure 5a). Conversely, the reacted corrosion film on the as-received surface stayed strongly anodic (although its current density decreased as its area increased), while the un-reacted surface film was strongly cathodic instead of neutral (Figure 5b).

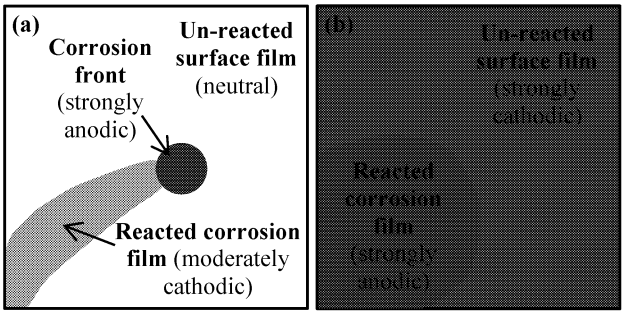

Figure 5. Schematic electrochemical surface profiles of (a) corroding acid-cleaned or mechanically-polished AZ31B surface (b) corroding as-received AZ31B surface with heavy metal surface contaminants.

It was determined that the acid-cleaning and mechanical polishing procedures both removed the Fe and Cu impurity particles originally present on the as-received surface. As shown in Table III, these two metals are strong cathodes with respect to Mg. It is, therefore, very likely that they were responsible for the local electrochemical differences that have been discussed.

Table III. Typical corrosion potentials of selected metal phases [First five phases determined in deaerated 5% NaCl solution saturated with $Mg(OH)_2$ (pH 10.5), testing solution for the last two phases not stated in the reference [1]

Metal Phase	E_{corr} (V_{SCE})
Mg	-1.65
Al_6Mn	-1.52
Al_4Mn	-1.45
Al_8Mn_5	-1.25
Al_8Mn_5(Fe)	-1.20
Fe	-0.50
Cu	-0.12

A schematic model of the corrosion processes occurring for polished or acid-cleaned AZ31B surfaces is presented in Figure 6; note that this is the same mechanism that was described by Williams et al. [11]. At the start of localized corrosion, only the native or unreacted surface film is present on the surface (Figure 6a). Al-Mn particles, which are commonly seen in AZ31 microstructures, are suspected to lie beneath the surface of the unreacted film. As localized corrosion proceeds, a dark reacted corrosion film replaces the original surface film (Figure 6b). Since only Mg metal is expected to be dissolved, the reacted corrosion film becomes enriched with Al-Mn intermetallic particles which are moderately cathodic (approximately 0.1 to 0.4 V nobler) with respect to Mg (refer to Table IV). As a result, the reacted corrosion film becomes cathodic with respect to the unreacted surface film and the location of anodic reaction (1) shifts to the unreacted film, directly adjacent to the reacted film. This electrochemical mechanism results in a lateral corrosion front movement and, therefore, closely resembles filiform corrosion.

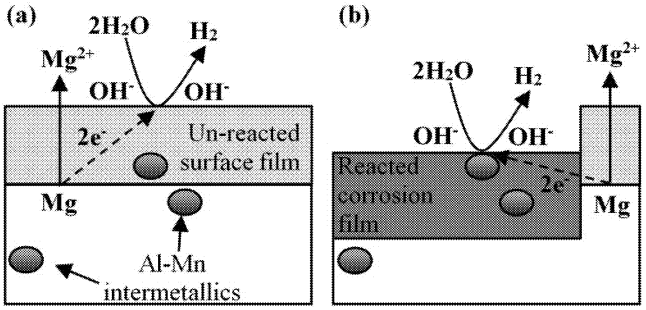

Figure 6. Schematic model of the localized corrosion processes occurring on an acid-cleaned or polished AZ31B surface.

A schematic model of the corrosion processes occurring for the as-received AZ31B with heavy metal contamination on the surface is presented in Figure 7. Intense microgalvanic activity between reactions (1) and (2) occurs due to the presence of noble Fe and Cu particles on the surface of the un-corroded areas. (Figure 7a). As localized corrosion proceeds, it is again expected that the reacted corrosion film will become enriched with Al-Mn intermetallics from the alloy microstructure (Figure 7b). However, it can be seen in Table III that Fe and Cu have corrosion potentials approximately 1.1 to 1.5 V nobler than Mg, which also makes them strongly cathodic with respect to each of the listed Al-Mn phases. Thus, since the heavy metal particles are present in both the reacted and unreacted areas of the film, the enrichment of Al-Mn particles in the reacted film is expected to be negligible in this case. Anodic reaction (1) will therefore continue to occur from underneath the reacted corrosion film, coupling with cathodic reaction (2) occurring on the unreacted surface film. This electrochemical mechanism results in a downward and lateral corrosion movement, which may resemble a mixture of pitting and filiform behavior.

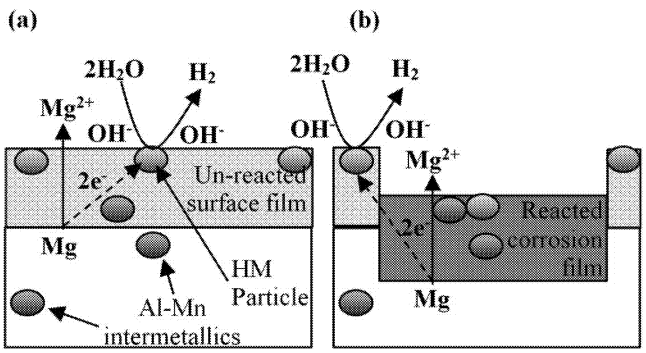

Figure 7. Schematic model of the localized corrosion processes occurring on an as-received AZ31B surface with heavy metal (HM) particle enrichment in the surface film.

Conclusion

The local electrochemical processes associated with filiform-like corrosion of Mg alloy AZ31B in 0.01 M NaCl solution were tracked using the scanning vibrating electrode technique (SVET). Changes in the electrochemical behavior occurred when altering the surface state of the alloy. SVET mapping of an as-received AZ31B surface showed intense microgalvanic activity that caused corrosion to occur in a downward direction as well as laterally. This was attributed to an enrichment of Fe and Cu heavy metal particles in the native oxide film. Acid-cleaning in 10% H_2SO_4 for 20 s and mechanical polishing of the as-received surface both appeared to successfully remove any strong cathodic contamination, since both of these surfaces displayed electrochemical activity that was more typical of filiform-like corrosion, as has been previously reported.

Acknowledgements

The authors would like to thank the Automotive Partnerships Canada (APC) program of the Natural Sciences and Engineering Council of Canada (NSERC) for financial support of this research.

References

1. G.L. Song and A. Atrens, "Understanding Magnesium Corrosion", *Adv. Eng. Mater.*, 5 (12) (2003), 837-858.

2. G.L. Makar and J. Kruger, "Corrosion of Magnesium", *Inter. Mater. Rev.*, 38 (3) (1993), 138-153.

3. P. Schmutz, V. Guillaumin, R.S. Lillard, J.A. Lillard and G.S. Frankel, "Influence of Dichromate Ions on Corrosion Processes on Pure Magnesium", *J. Electrochem. Soc.*, 150 (4) (2003), B99-B110.

4. C.R. McCall, M.A. Hill and R.S. Lillard, "Crystallographic Pitting in Magnesium Single Crystals", *Corros. Engineer., Sci. Technol.*, 40 (4) (2005), 337-343.

5. G. Williams and R. Grace, "Chloride-Induced Filiform Corrosion of Organic-Coated Magnesium", *Electrochim. Acta,* 56 (2008), 1894-1903.

6. O. Lunder, J.E. Lein, S.M. Hesjevik, T.Kr. Aune, and K. Nisancioglu, "Filiform Corrosion of a Magnesium Alloy," 11th Annual Corrosion Congress, Florence, Italy, 1990, 5.255–5.262.

7. G.Williams, H.L. Dafydd and R. Grace, "The Localised Corrosion of Mg Alloy AZ31 in Chloride Containing Electrolyte studied by a Scanning Vibrating Electrode Technique", *Electrochim. Acta,* 109 (2013), 489-501.

8. E.A. Nyberg, A.A. Luo, K. Sadayappan and W. Shi, "Magnesium for Future Autos", *Adv. Mater. Process.*, 166 (10) (2008), 35-37.

9. B.E. Carlson, R. Verma, W. Yuan and R.T. Szymanski, "Friction Stir Welding of a Magnesium AZ31 Sub-Assembly", (Paper presented at Sheet Metal Welding Conference XV, Livonia, MI, 2012).

10. S. Rossi, M. Fedel, F. Deflorian, M. Vadillo, "Localized Electrochemical Techniques: Theory and Practical Examples in Corrosion Studies", *C.R. Chimie*, 11 (2008), 984-994.

11. G. Williams and H.N. McMurray, "Localized Corrosion of Magnesium in Chloride-Containing Electrolyte Studied by a Scanning Vibrating Electrode Technique", *J. Electrochem. Soc.*, 155 (7) (2008), C340-C349.

12. X.R. Zhang, Z.P. Cano, B.M. Wilson, J.R. Kish and J.R. McDermid, "Corrosion Behavior of Friction Stir Welded Mg Alloy Joints for Automotive Applications" (Paper presented at Materials Science and Technology 2013, Montreal, Canada, 2013).

13. G.L. Song, Z. Xu, "The Surface, Microstructure and Corrosion of Magnesium Alloy AZ31 Sheet", *Electrochim. Acta*, 55 (2010), 4148-4161.

14. U.C. Nwaogu, C. Blawert, N. Scharnagl, W. Dietzel and K.U. Kainer, "Influence of Inorganic Acid Pickling on the Corrosion Resistance of Magnesium Alloy AZ31 Sheet", *Corros. Sci*, 51 (2009), 2544-2556.

15. R. Walter and M.B. Kannan, "Influence of Surface Roughness on the Corrosion Behavior of Magnesium Alloy", *Mater.Design*, 32 (2011), 2350-2354.